Article

Cell Reports

Mdm2 Phosphorylation Regulates Its Stability and Has Contrasting Effects on Oncogene and Radiation-Induced Tumorigenesis

Graphical Abstract

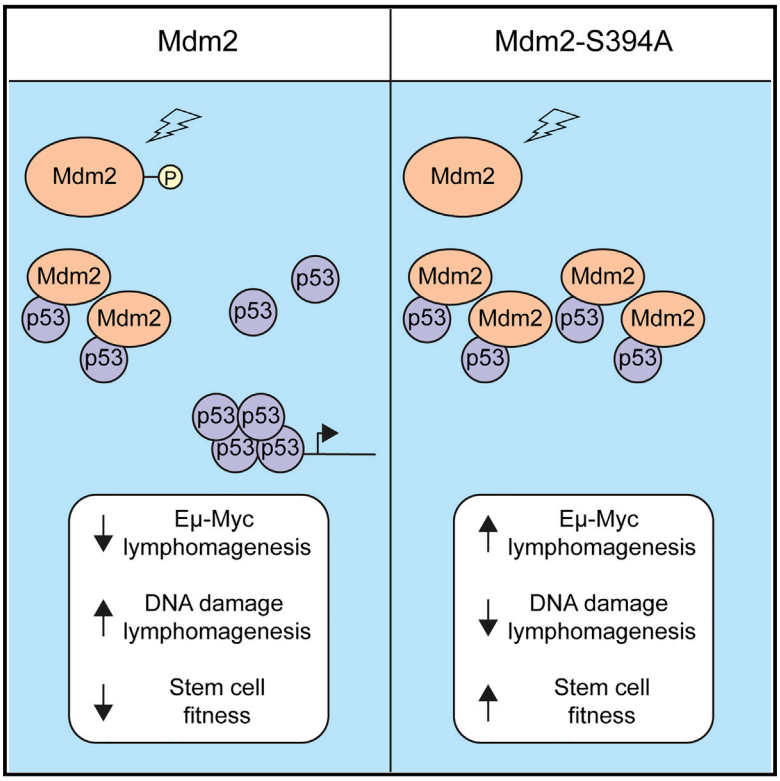

Authors

Michael I. Carr, Justine E. Roderick, Hugh S. Gannon, Michelle A. Kelliher, Stephen N. Jones

Correspondence

stephen.jones@umassmed.edu

In Brief

Carr et al. find that phosphorylation of Mdm2 at a single residue (S394) by ATM destabilizes the protein and can alter hematopoietic stem cell fitness. Furthermore, this phosphorylation event promotes or suppresses lymphomagenesis in mice, depending upon the nature of the oncogenic stress.

Highlights

- ATM phosphorylation of Mdm2 regulates p53-mediated DDR by altering Mdm2 stability
- Mdm2-S394 phosphorylation promotes p53 suppression of Myc-induced lymphomagenesis
- Mdm2-S394 phosphorylation inhibits p53 suppression of IR-induced lymphomagenesis
- Mdm2 phosphorylation regulates radiation-induced BM failure by governing HSC fitness

Carr et al., 2016, Cell Reports *16*, 2618–2629
September 6, 2016
http://dx.doi.org/10.1016/j.celrep.2016.08.014

OPEN ACCESS
CellPress

Cell Reports
Article

Mdm2 Phosphorylation Regulates Its Stability and Has Contrasting Effects on Oncogene and Radiation-Induced Tumorigenesis

Michael I. Carr,[1] Justine E. Roderick,[2] Hugh S. Gannon,[1] Michelle A. Kelliher,[2] and Stephen N. Jones[1,2,3,*]
[1]Department of Cell and Developmental Biology
[2]Department of Molecular, Cell and Cancer Biology
University of Massachusetts Medical School, Worcester, MA 01655, USA
[3]Lead Contact
*Correspondence: stephen.jones@umassmed.edu
http://dx.doi.org/10.1016/j.celrep.2016.08.014

SUMMARY

ATM phosphorylation of Mdm2-S394 is required for robust p53 stabilization and activation in DNA-damaged cells. We have now utilized *Mdm2*^{S394A} knockin mice to determine that phosphorylation of Mdm2-S394 regulates p53 activity and the DNA damage response in lymphatic tissues in vivo by modulating Mdm2 stability. Mdm2-S394 phosphorylation delays lymphomagenesis in *Eμ-myc* transgenic mice, and preventing Mdm2-S394 phosphorylation obviates the need for p53 mutation in Myc-driven tumorigenesis. However, irradiated *Mdm2*^{S394A} mice also have increased hematopoietic stem and progenitor cell functions, and we observed decreased lymphomagenesis in sub-lethally irradiated *Mdm2*^{S394A} mice. These findings document contrasting effects of ATM-Mdm2 signaling on p53 tumor suppression and reveal that destabilizing Mdm2 by promoting its phosphorylation by ATM would be effective in treating oncogene-induced malignancies, while inhibiting Mdm2-S394 phosphorylation during radiation exposure or chemotherapy would ameliorate bone marrow failure and prevent the development of secondary hematological malignancies.

INTRODUCTION

It is widely accepted that the p53 tumor suppressor protein functions primarily as a transcription factor, capable of promoting or repressing the transcription of a multitude of genes (Beckerman and Prives, 2010). Proper coordination of p53-responsive gene expression plays an important role in tumor suppression, as evidenced by the rapid development of tumors in mice lacking p53 (Donehower et al., 1992) and by the fact that most human cancers harbor mutations in p53 or in key regulators of p53 signaling (Soussi and Béroud, 2001). The tumor suppressive capacity of p53 has been traditionally attributed to its ability to inhibit cell proliferation or promote apoptosis, as limiting or eliminating cells bearing genetic lesions would obviously prevent the propagation and accumulation of genetic errors and the formation or progression of tumorigenesis. However, p53 tumor suppressive mechanisms distinct from p53-mediated growth arrest and apoptosis have been recently proposed, suggesting an even broader contribution of p53 activities to tumor suppression (Brady et al., 2011; Li et al., 2012).

Because deregulated growth arrest and apoptosis is detrimental to embryogenesis and normal cell growth, the activities of p53 are strictly regulated in non-damaged cells and tissues. Basal levels of p53 are low, and this transcription factor is largely inactive under homeostatic conditions. In contrast, p53 is rapidly stabilized and activated in response to a multitude of stresses, including activated oncogenes, hypoxia, ribosomal stress, and DNA damage. The chief negative regulator of p53 stabilization and activity is the Mdm2 oncoprotein, which can bind and mask the transactivation domain of p53 and function as an E3 ubiquitin ligase capable of directing p53 nuclear export and proteosomal degradation (Momand et al., 1992; Oliner et al., 1993; Haupt et al., 1997; Honda et al., 1997; Kubbutat et al., 1997). The central role of Mdm2 in regulating p53 activity is best illustrated by studies using Mdm2-conditional mouse models that identified roles for Mdm2 in regulating p53-dependent cell growth arrest or apoptosis in various tissues (Gannon and Jones, 2012) and p53-dependent lethality of Mdm2 null mice during early embryogenesis (Jones et al., 1995; Montes de Oca Luna et al., 1995).

Similar to Mdm2, the homologous protein MdmX (Mdm4) is also capable of binding p53 and inhibiting p53 transactivation of target genes (Shvarts et al., 1996), and mice null for *MdmX* display a similar p53-dependent embryonic lethality, albeit at a slightly later time during development (Parant et al., 2001; Migliorini et al., 2002). Unlike Mdm2, MdmX does not possess the ability to directly ubiquitinate p53 (Jackson and Berberich, 2000). However, Mdm2 and MdmX have been shown to interact via their C-terminal RING domains, and this heterodimerization promotes maximal Mdm2 E3 ligase activity toward p53 (Tanimura et al., 1999; Sharp et al., 1999, Kawai et al., 2007). Recently, a series of Mdm2 and MdmX knockin mouse models have been generated that display altered Mdm2-MdmX interactions or Mdm2 E3 ligase activity (Itahana et al., 2007; Pant et al.,

2011; Huang et al., 2011; Tollini et al., 2014). Analyses of these various models have revealed that Mdm2-MdmX interactions are critical in inhibiting p53 activity during development and tissue homeostasis, whereas the E3 ligase function of Mdm2 is critical in regulating p53 protein and activity levels in cellular and organismal response to DNA damage (Tollini et al., 2014).

Inhibition of p53 levels and activities by MDM proteins must be interrupted in order for p53 to become elevated and activated in response to DNA damage or other forms of stress (Meek, 2015). During the DNA damage response (DDR), Mdm2-p53 signaling is mediated by DNA-damage-activated kinases such as ATM (ataxia telangiectasia mutated). Upon sensing double-stranded DNA breaks, the PI3K-related ATM becomes activated and directly or indirectly induces phosphorylation of a multitude of proteins involved in the damage response, including p53, Mdm2, and MdmX (Shieh et al., 1997, 2000; Maya et al., 2001; Pereg et al., 2005; Chen et al., 2005). Initial biochemical and cell-based studies suggested that ATM-mediated phosphorylation of two key residues on p53, Ser18 and Ser23 (human Ser15 and Ser20), could account for p53 stabilization and activation following DNA damage. However, analysis of genetically engineered mouse models revealed that these phosphorylation events were insufficient to account for the full effects of DNA damage on Mdm2-p53 signaling or p53 tumor suppression (Wu et al., 2002; Chao et al., 2003, 2006; Sluss et al., 2004). We have previously reported the generation and initial characterization of a mouse model (*Mdm2*^{S394A} mice), wherein ATM phosphorylation of Mdm2 at serine residue 394 was abolished (Gannon et al., 2012). Cells and tissues in *Mdm2*^{S394A} mice display profound defects in DNA-damage-induced p53 protein stabilization and p53 target gene activation. This failure to induce a robust p53 response translates to less p53-dependent apoptosis in hematopoietic tissues, radioresistance, and increased spontaneous lymphomagenesis. Regulation of the amplitude and duration of the p53-induced DDR in *Mdm2*^{S394A} cells and mice underscores the importance of ATM phosphorylation of Mdm2 in the DDR.

Several in vitro studies have suggested that ATM phosphorylation of Mdm2 governs p53 stability and/or activity following DNA damage by regulating p53 degradation and nuclear export, Mdm2 autodegradation, and Mdm2 oligomerization and E3 processivity (Maya et al., 2001; Stommel and Wahl, 2004; Cheng et al., 2009). In our present study, we explore in vivo the mechanism by which Mdm2 phosphorylation alters p53 functions in a radiosensitive tissue. Furthermore, we have sought to address whether ATM-Mdm2-p53 signaling in mice impacts tumorigenesis induced by activated oncogenes or ionizing radiation (IR), and we explore the role of ATM-Mdm2 signaling in promoting IR-mediated bone marrow failure. Our results indicate that Mdm2 phosphorylation has dramatically different, stress-dependent effects in tumorigenesis.

RESULTS

ATM-Mdm2 Signaling Regulates the p53 Response in Lymphatic Tissues

To further explore the effects of Mdm2 Ser394 phosphorylation on p53 protein levels and activity in vivo, we analyzed thymi of mice treated with a low dose (1.75 Gy) of IR. Although p53 protein levels were elevated in the thymus of *Mdm2*^{S394A} mice at 3 hr and 6 hr following IR, there was considerably less total p53 protein and phosphorylated p53 (S18) in treated *Mdm2*^{S394A} mice than in irradiated wild-type (WT) mice (Figure 1A). This is similar to what we observed previously in these mice using higher dosages of IR (Gannon et al., 2012). However, we also noted that basal levels of p53 appeared slightly lower in *Mdm2*^{S394A} thymi than in WT thymi, and more Mdm2 protein appeared to be present in *Mdm2*^{S394A} thymi in absence of acute DNA damage and following IR treatment (Figure 1A). There was a significant decrease in WT Mdm2 protein levels in whole thymus following DNA damage, an observation that has been made in cell culture settings by several groups (Stommel and Wahl, 2004; Itahana et al., 2007; Inuzuka et al., 2010; Malonia et al., 2015). However, Mdm2 protein levels appeared to diminish after IR at a lesser rate in *Mdm2*^{S394A} thymus than in WT thymus. To more definitively quantify the observed differences in thymic Mdm2 and p53 levels, we analyzed biological triplicates of untreated and irradiated WT and *Mdm2*^{S394A} thymi. This confirmed that Mdm2 protein levels were higher in *Mdm2*^{S394A} thymi both before and after treatment and that the IR-induced relative decrease in Mdm2 protein levels was far less in *Mdm2*^{S394A} thymi (Figure 1B). In contrast, the reduction of MdmX levels induced by DNA damage (Wang et al., 2009) appears to be similar in WT and *Mdm2*^{S394A} thymi. Though not statistically significant, p53 levels are slightly lower in untreated *Mdm2*^{S394A} thymi (Figure 1B, bottom) and are significantly lower in irradiated *Mdm2*^{S394A} thymi. Although p53 target gene expression was similar in non-damaged WT and *Mdm2*^{S394A} thymi (Figure 1C), a reduction in IR activation of p53 target genes was seen in *Mdm2*^{S394A} thymi. Reduced expression levels of *Mdm2*, the cell-cycle regulator *Cdkn1a* (p21), and the pro-apoptotic genes *Puma*, *Noxa*, and *Bax* are in agreement with reduced levels of p21, Puma, and cleaved Caspase-3 protein (Figure 1A) and with a clear reduction in DNA-damage-induced apoptosis in *Mdm2*^{S394A} thymi following exposure of mice to low-level IR (Figure 1D).

To explore whether these effects were unique to the thymus, we also examined protein levels in spleens of WT and *Mdm2*^{S394A} mice. As observed in the thymus, there appeared to be less total p53 in *Mdm2*^{S394A} spleens before and after irradiation (Figure S1), and Mdm2 levels were higher in both untreated and irradiated *Mdm2*^{S394A} spleens. Intriguingly, while no induction of Mdm2 protein was observed in thymi of WT and *Mdm2*^{S394A} mice in response to IR, spleens of both genotypes displayed a more "classic" induction of Mdm2 often seen in cultured cells after genotoxic stress. Similar to what was observed in the thymus, decreased levels of p53 and increased levels of Mdm2 in irradiated *Mdm2*^{S394A} spleens correlate with reduced p53 activation (phospho-S18 p53), reduced levels of Puma and p21, and reduced levels of cleaved Caspase-3 (Figure S1).

ATM Phosphorylation of Mdm2-S394 Governs Mdm2 Levels and Stability

In order to directly analyze the effects of Mdm2-S394 phosphorylation on the stability of Mdm2 in the presence and absence of

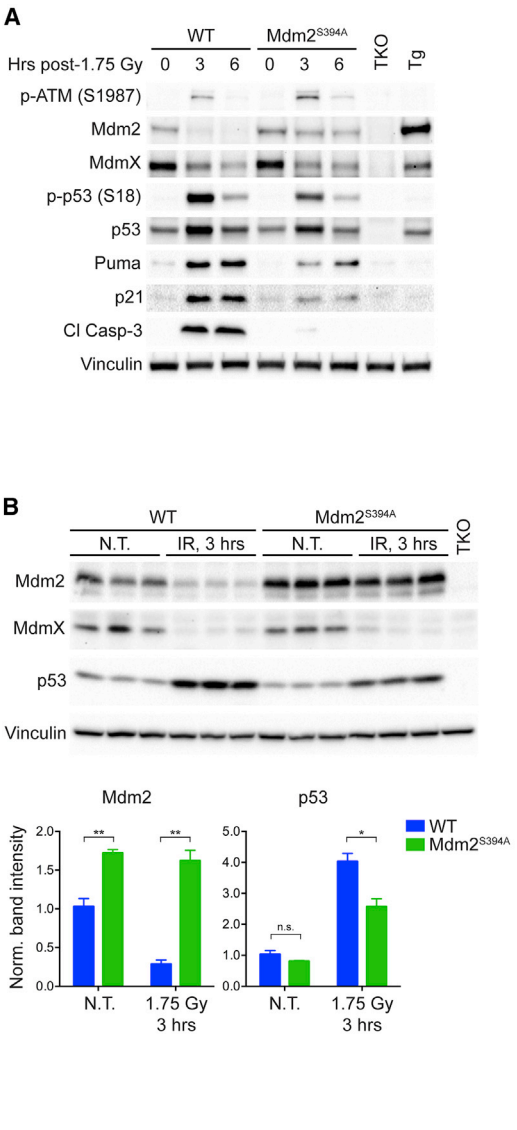

Figure 1. ATM Phosphorylation of Mdm2-S394 Regulates Mdm2 Levels and p53 Activity

(A) WT and *Mdm2*^{S394A} mice were left untreated or exposed to 1.75 Gy ionizing radiation (IR), and thymi were harvested at 3 and 6 hr. Protein levels were analyzed by western blotting. TKO indicates *Mdm2*$^{-/-}$, *MdmX*$^{-/-}$, and *p53*$^{-/-}$ control; Tg indicates *Mdm2*$^{Tg/+}$ Mdm2 overexpressing control.

(B) Thymus protein levels of biological triplicates of WT and *Mdm2*^{S394A} mice left untreated or treated as in (A) for 3 hr were analyzed by western blotting. Band intensities were determined by densitometry. Mdm2 and p53 levels were normalized for Vinculin levels and average values plotted (±SEM). *$p < 0.05$, **$p < 0.01$ (Student's t tests).

(C) Mice were treated as in (A), and fold expression of p53-target genes was determined by real-time qPCR, relative to untreated WT samples using *Rplp0* as internal reference (n = 3, ± SEM). *$p < 0.05$, **$p < 0.01$ (Student's t tests).

(D) TUNEL staining of thymi from mice treated as in (A). Scale bars represent 100 μm.

exogenous DNA damage, we measured the half-life of Mdm2 proteins using the protein synthesis inhibitor cycloheximide. Although basal levels of Mdm2 transcription are similar in WT and *Mdm2*^{S394A} thymi, Mdm2 protein levels are elevated in non-damaged *Mdm2*^{S394A} mice (Figures 1A and 1B), suggesting that the mutant Mdm2 protein is more stable in the absence of exogenous DNA damage. However, we observed no significant difference in the half-lives of WT Mdm2 and Mdm2^{S394A} in untreated thymocytes (80 and 65 min, respectively, overlapping 95% confidence intervals) (Figure 2A). But following treatment of the thymocytes with 2.5 Gy IR, the half-life of WT Mdm2 decreased by more than 50% (29 min), whereas the half-life of Mdm2^{S394A} remained unchanged (69 min) (Figure 2B). These data show that phosphorylation of Mdm2-S394 by ATM is a crucial event in DNA-damage-induced destabilization of Mdm2 under physiological conditions. As previous studies have shown ATM phosphorylation of Mdm2 to impact the ability of Mdm2 to promote p53 degradation (Maya et al., 2001; Cheng et al., 2009, 2011), we also examined whether p53 stability was affected in the presence and absence of DNA damage. We observed no difference in the half-life of p53 in non-treated WT versus *Mdm2*^{S394A} thymocytes (Figure S2A). As expected, DNA damage stabilized p53 levels in WT cells (Figure S2B). Likewise, DNA damage stabilized p53 levels in *Mdm2*^{S394A} thymocytes, albeit to a lower level than seen in WT thymocytes.

Since we observed no difference in the rate of p53 decay in *Mdm2*^{S394A} and WT thymocytes, it is possible that phosphorylation of Mdm2-S394 upregulates p53 activity not only by altering p53 protein stability but also by inhibiting Mdm2-p53 complex formation and Mdm2-mediated steric inhibition of p53 transcriptional activation. Therefore, we examined the effects of Mdm2-S394 phosphorylation on Mdm2-p53 binding in the presence and absence of DNA damage in whole tissue extracts. In an effort to control for potential differences in antibody affinity following IR-induced modification of Mdm2, Mdm2 was immunoprecipitated from untreated and irradiated thymus lysates in separate experiments with two distinct antibodies whose epitopes reside in opposing termini of Mdm2 (Figure 2C, left). In both cases, more p53 co-immunoprecipitated with Mdm2^{S394A} than WT Mdm2 in untreated thymi, whereas similar amounts of p53 co-immunoprecipitated with Mdm2 in irradiated *Mdm2*^{S394A} and WT thymi. As there was less p53 observed in the total lysates of untreated and irradiated *Mdm2*^{S394A} thymi relative to WT thymi (Figure 2C, right), this result reveals increased levels of Mdm2-bound p53 (relative to total p53) in undamaged and IR-treated *Mdm2*^{S394A}

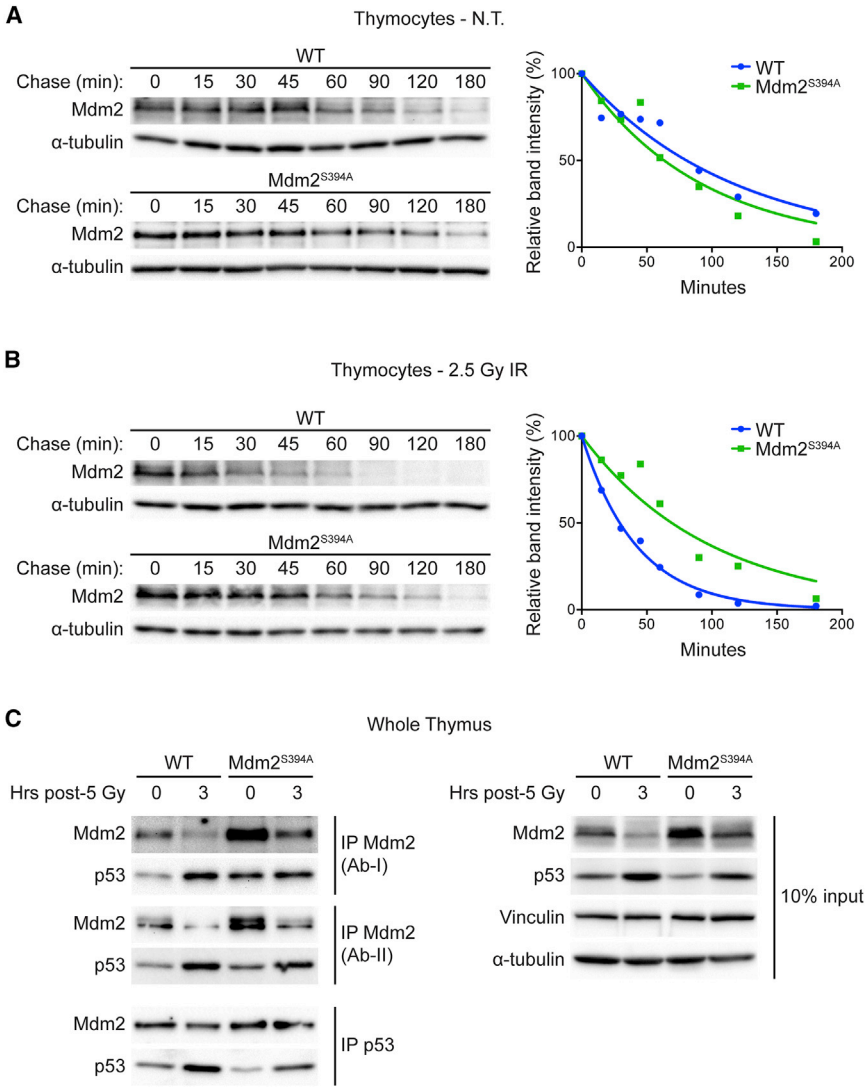

Figure 2. ATM Phosphorylation of Mdm2-S394 Regulates Mdm2 Stability and Levels of Mdm2-Bound p53

(A) Thymocytes harvested from WT and *Mdm2*^{S394A} mice (n = 6) were treated with 100 μg/ml cycloheximide and harvested at the indicated time points. The levels of Mdm2 and α-tubulin were analyzed by western blotting. Band intensities were determined by densitometry, and Mdm2 levels normalized to α-tubulin were plotted. One-phase decay curves were fitted using GraphPad Prism software.

(B) Thymocytes harvested from WT and *Mdm2*^{S394A} mice (n = 6–8) were exposed to 2.5 Gy IR and treated as in (A).

(C) Thymus protein extracts from mice untreated or exposed to 5 Gy IR were immunoprecipitated with antibodies for Mdm2 (NBP1-02158 (Ab-I) and Ab-5 (Ab-II)) and p53. Immunoprecipitates were analyzed by western blotting for Mdm2 and p53. Total lysate (10% input) was analyzed by western blotting.

thymi. We confirmed this finding by performing the reciprocal experiment using p53 immunoprecipitation, and observed that equivalent amounts of Mdm2 co-immunoprecipitated with lesser amounts of p53 in untreated and irradiated *Mdm2*^{S394A} thymi. Additional immunoprecipitation experiments against MdmX detected no effect on the relative amounts of Mdm2-bound MdmX or p53-bound MdmX before or after DNA damage (Figure S3).

Collectively, these data reveal that phosphorylation of Mdm2-S394 under basal conditions and following acute IR exposure reduces Mdm2 stability, thereby reducing the relative amount of Mdm2-bound p53. This reduction in Mdm2-p53 complex negatively impacts Mdm2 inhibition of p53 target gene transactivation as well as Mdm2 destabilization of p53.

Accelerated *Eμ-myc* Driven Lymphomagenesis in *Mdm2*^{S394A} Mice

We have previously described an increased susceptibility to spontaneous tumorigenesis in *Mdm2*^{S394A} mice (Gannon et al., 2012). We next sought to examine the effects of Mdm2-S394 phosphorylation on oncogene-induced tumorigenesis. *Mdm2*^{S394A} mice were bred to *Eμ-myc* transgenic mice to generate *Eμ-myc* and *Eμ-myc; Mdm2*^{S394A} mice. *Eμ-myc* mice succumb to pre-B/B cell lymphomas within 3–6 months of age. We observed a median time to tumor presentation of 126 days in *Eμ-myc* mice, consistent with previous studies (Adams et al., 1985; Eischen et al., 1999; Sluss et al., 2010) (Figure 3A). In contrast, the median time to tumor presentation in *Eμ-myc; Mdm2*^{S394A} mice was only 71 days. This represents a nearly 50% reduction in the time to Myc-induced tumorigenesis when ATM phosphorylation of Mdm2-S394 is inhibited. All tumor-bearing *Eμ*-myc mice and *Eμ-myc; Mdm2*^{S394A} mice presented with enlarged lymph nodes and spleens, and representative tumors were examined histologically by H&E staining. Both genotypes developed similar, high-grade lymphomas, composed of monotonous populations of pre-B/B cells. Tumors displayed high levels of mitosis and apoptosis and the characteristic ''starry-sky'' pattern resultant from abundant tingible body-laden macrophages. The cell type was further confirmed by immunohistochemistry (IHC) through positive staining for B220/CD45R (Figure 3B).

Myc-driven B cell tumors face selective pressure to inactivate the p53 pathway through p53 mutation, Mdm2 overexpression, or by loss of Arf (Eischen et al., 1999). We examined the status of p53, Mdm2, and Arf in a panel of 10 tumors that developed in *Eμ-myc;Mdm2*^{S394A} mice (Figure 3C). No marked differences in p53 protein levels were observed in any of the 10 tumors examined. However, Arf levels appeared more variable, with loss of detectable Arf protein seen in 4 of the 10 tumors. RT-PCR confirmed that three of those four tumors did not express

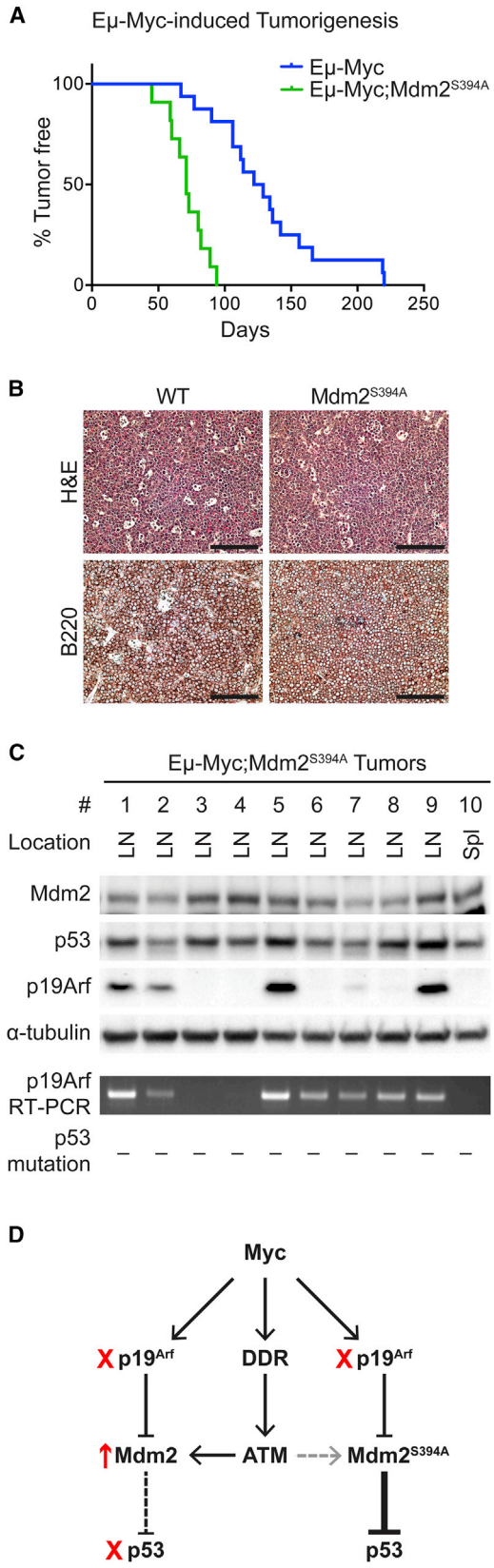

Figure 3. Accelerated *Eμ-myc* Driven Lymphomagenesis in *Mdm2*^{S394A} Mice

(A) Kaplan-Meier survival curves of *Eμ-Myc* (n = 16) and *Eμ-Myc;Mdm2*^{S394A} (n = 11) mice. Median survival times were as follows: *Eμ-Myc* (125.5 days) and *Eμ-Myc;Mdm2*^{S394A} (71 days). Curves were compared by log rank test: $p < 0.0001$.

(B) Representative B cell lymphomas in lymph nodes of *Eμ-Myc* (98 days) and *Eμ-Myc;Mdm2*^{S394A} (80 days) mice were stained by H&E (top) and with an antibody specific for B220 (bottom). Scale bars represent 100 μm.

(C) The levels of Mdm2, p53, and Arf were analyzed by western blotting in a panel of *Eμ-Myc;Mdm2*^{S394A} tumors. RT-PCR confirmed that full-length *Arf* message was absent in 3 of 10 tumors (second from bottom). *p53* cDNA was sequenced for each tumor, revealing no mutations (bottom). LN, lymph node; Spl, spleen.

(D) Schematic outlining the proposed methods of p53 activation by Myc. Tumors in mice in which Mdm2 is WT select for loss of Arf or p53, or Mdm2 overexpression (Eischen et al., 1999). We propose that *Mdm2*^{S394A} mice obviate the need for p53 loss or Mdm2 overexpression by mitigating the effects of the DDR arm of Myc signaling to p53.

full-length Arf mRNA. Arf levels have been shown previously to be elevated in cases where p53 is mutant and the negative feedback loop between p53 and Arf is disrupted, and we identified several tumors wherein Arf appeared to be increased. However, sequencing of the entire p53 coding sequence of all 10 tumors revealed no mutations in p53 gene transcripts. Thus, the observed variability in Arf levels within the Myc tumors was not a result of p53 status. Furthermore, Mdm2 protein levels did not vary significantly between tumors, and qPCR analysis also failed to detect alterations in *Mdm2* transcript levels in any tumor (data not shown). Thus, ATM phosphorylation of Mdm2-S394 strongly suppresses Myc oncogene-induced tumorigenesis in mice, and inhibition of this signaling event obviates the need for mutation of the Mdm2-p53 tumor suppressor axis in Myc-driven B cell lymphomagenesis (Figure 3D).

Mdm2^{S394A} Mice Are Resistant to IR-Induced Lymphomagenesis

We next sought to examine the effects of ATM phosphorylation of Mdm2-S394 on IR-induced tumorigenesis. Exposure of mice to repeated low-dose IR promotes the development of thymic lymphomas (Kaplan and Brown, 1952). This lymphomagenesis is significantly enhanced in the absence of p53 (Kemp et al., 1994; Labi et al., 2010; Michalak et al., 2010). As we have shown that IR-induced p53 activity is diminished in both the thymus and spleen of *Mdm2*^{S394A} mice, we anticipated a heightened sensitivity to IR-induced lymphomagenesis in this model. Cohorts of WT, *Mdm2*^{S394A}, *p53*$^{+/-}$, and *p53*$^{-/-}$ mice were subjected to four weekly doses of 1.75 Gy IR and monitored over time for tumor presentation. 89% of WT mice developed lymphomas by 400 days, with a median survival of 197 days (Figure 4A), consistent with a previous study employing this dosing strategy (Labi et al., 2010). Also consistent with previous studies was the significant acceleration of lymphomagenesis observed in the absence of p53 (Kemp et al., 1994; Labi et al., 2010; Michalak et al., 2010). All *p53*$^{-/-}$ mice developed lymphomas within 151 days, with a median survival of 131 days, whereas all *p53*$^{+/-}$ mice developed lymphomas within 167 days, with a median survival of 154 days. Surprisingly, *Mdm2*^{S394A} mice proved to be highly resistant to IR-induced

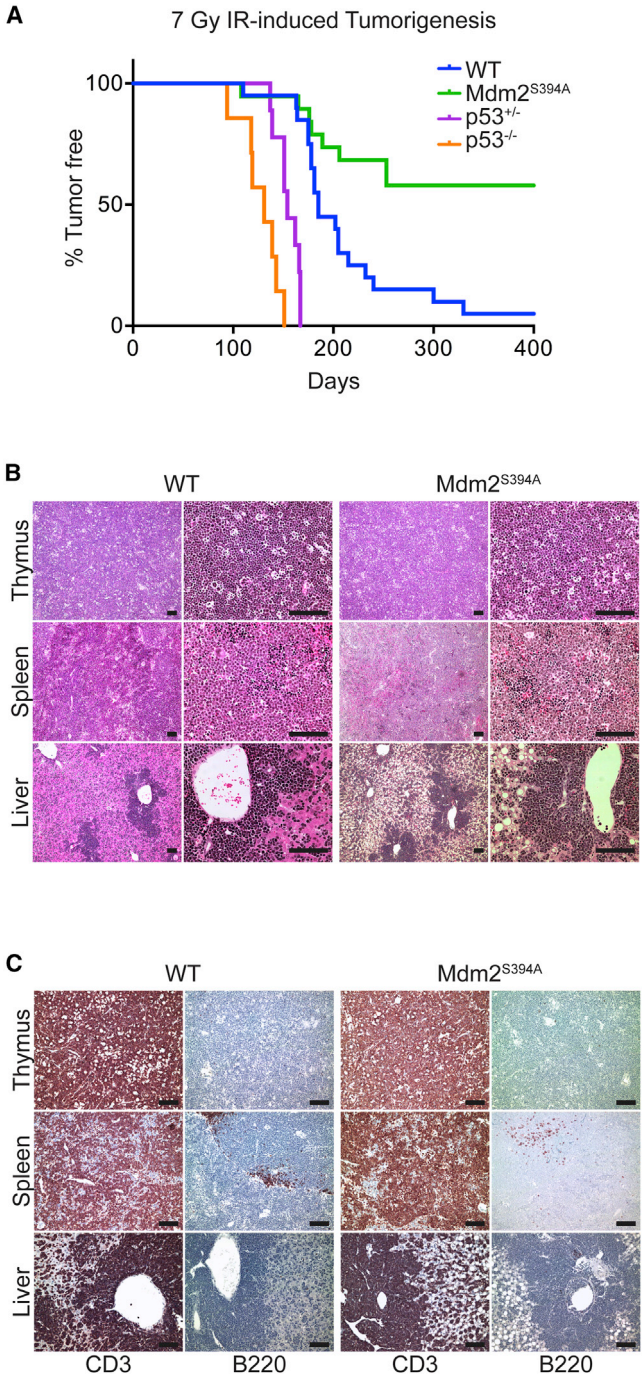

Figure 4. *Mdm2*^{S394A} Mice Are Resistant to IR-Induced Lymphomagenesis

(A) Kaplan-Meier survival curves of WT (n = 20), *Mdm2*^{S394A} (n = 19), *p53*$^{+/-}$ (n = 9), and *p53*$^{-/-}$ (n = 7) mice exposed to 7 Gy cumulative IR. Median survival times were as follows: WT (185 days), *Mdm2*^{S394A} (n.d.), *p53*$^{+/-}$ (154 days), and *p53*$^{-/-}$ (131 days). Curves were compared by log rank test: WT to *p53*$^{-/-}$ ($p < 0.0001$), WT to *p53*$^{+/-}$ ($p < 0.0001$), WT to *Mdm2*^{S394A} ($p = 0.0007$), *Mdm2*^{S394A} to *p53*$^{+/-}$ ($p < 0.0001$), and *Mdm2*^{S394A} to *p53*$^{-/-}$ ($p < 0.0001$).

(B) Representative tissue sections of lymphomas that developed in the thymus, spleen, and liver of WT and *Mdm2*^{S394A} mice stained with H&E at 10× (left) and 40× (right) magnification. Scale bars represent 100 μm.

(C) Representative tissue sections of lymphomas that developed in the thymus, spleen, and liver of WT and *Mdm2*^{S394A} mice were stained with antibodies specific for CD3 (left) and B220 (right). Scale bars represent 100 μm. See also Figure S4.

thymic lymphomagenesis. Although tumor presentation in *Mdm2*^{S394A} mice followed similar initial kinetics as observed in WT mice, only 42% of *Mdm2*^{S394A} mice developed lymphoma, with a median survival among tumor-bearing mice of 184 days. Tumor-bearing animals presented with profoundly enlarged thymi, as well as frequent splenomegaly and hepatomegaly. Histological analyses of H&E stained tissues showed disorganized, hyperplastic lymphatic tissues as well as significant lymphocyte infiltration in portal regions of the liver (Figure 4B). IHC confirmed that the lymphomas arising in IR-treated mice were T-cell-derived, with positive staining for CD3 and negative staining for B220 (Figures 4C and S4). Thus, in contrast to their increased rate of spontaneous and oncogene-induced tumorigenesis, *Mdm2*^{S394A} mice are actually more resistant to radiation-induced T cell lymphomagenesis than WT mice, despite having clear defects in p53-mediated thymic apoptosis.

Radiation Resistance in *Mdm2*^{S394A} Mice Is Dictated by Improved Bone Marrow Recovery after IR

We have previously reported that *Mdm2*^{S394A} mice are resistant to threshold-lethal doses (8 Gy) of radiation. To better understand why ATM phosphorylation of Mdm2-S394 would promote radiation-induced lymphomagenesis yet provide resistance to acute radiation, we decided to examine further the response of these mice to whole-body IR. The primary cause of lethality in mice subjected to IR doses as high as 10 Gy is a p53-dependent ablation of the bone marrow compartment, known as hematopoietic syndrome (Komarova et al., 2004). Previous reports have revealed that even small changes in p53 activity can profoundly impact the hematopoietic system (Mendrysa et al., 2003; Terzian et al., 2007; Wang et al., 2011; Pant et al., 2013), and hematopoietic failure phenotypes have previously been described in mice bearing hypomorphic or reduced copies of functional *Mdm2* alleles (Mendrysa et al., 2003; Terzian et al., 2007). Furthermore, several p53 target genes, including those encoding p21 or Puma, have been implicated in governing the radiosensitivity of murine bone marrow (Cheng et al., 2000; van Os et al., 2007; Shao et al., 2010; Yu et al., 2010; Wang et al., 2011; Pant et al., 2013).

To elucidate the basis for the acute radioresistance of *Mdm2*^{S394A} mice, we examined the expression of the p53-target genes *Mdm2*, *p21*, *Puma*, and *Noxa* by qPCR in the bone marrow of WT, *Mdm2*^{S394A}, and *p53*$^{-/-}$ mice before and after irradiation (Figure 5A). As we observed in the thymus, no differences were present in the expression levels of any of the examined p53 target genes in untreated *Mdm2*^{S394A} bone marrow. Similar expression levels of the target genes were observed in untreated *p53*$^{-/-}$ mice. Following whole-body treatment of mice with 5 Gy IR, the expression levels of all four genes increased dramatically in WT bone marrow, indicative of a strong p53 response. However, lower levels of *p21*, *Puma*, and *Noxa* transcripts were detected in *Mdm2*^{S394A} bone marrow, indicating reduced p53

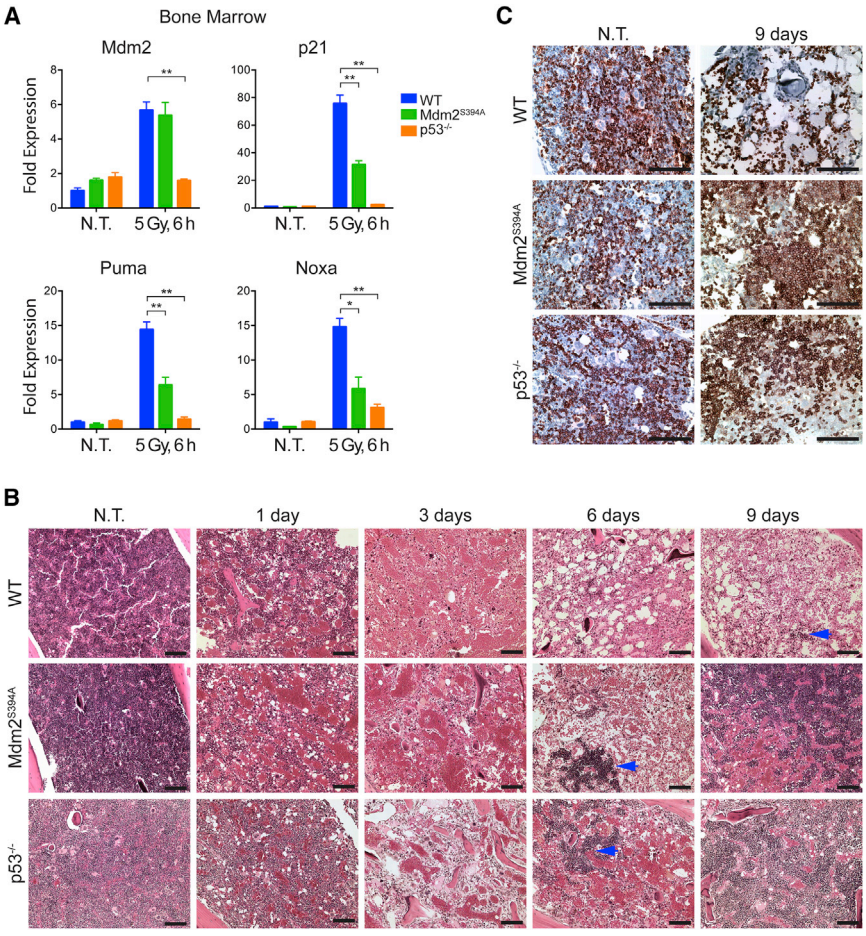

Figure 5. Threshold-Lethal Radiation Resistance in *Mdm2*^{S394A} Mice Is Dictated by Improved Bone Marrow Recovery following IR

(A) Fold expression of p53-target genes in bone marrow of WT, *Mdm2*^{S394A}, and *p53*$^{-/-}$ mice, untreated and 6 hr after 5 Gy IR, was determined by real-time qPCR. Fold expression was calculated relative to untreated WT samples using *Rplp0* as internal reference (n = 3–4 mice, ± SEM). *p < 0.05, **p < 0.01 (Student's t tests of ΔΔCt values).

(B) H&E stained bone marrow from WT, *Mdm2*^{S394A}, and *p53*$^{-/-}$ mice exposed to 8 Gy IR. Blue arrows indicate nascent hematopoietic cell colonies. Scale bars represent 100 μm.

(C) Bone marrow sections from untreated and 9 days post-IR mice described in (B) were stained with an antibody specific for TER-119. Scale bars represent 100 μm.

activity in this tissue. Although *Mdm2* transcript levels did not appear to be overtly reduced in irradiated *Mdm2*^{S394A} bone marrow, no induction of *Mdm2*, *p21*, or *Puma* transcription was observed in the bone marrow of p53-deficient mice, pointing to the p53 dependence of their induction following irradiation.

We next examined the bone marrow of WT, *Mdm2*^{S394A}, and *p53*$^{-/-}$ mice by H&E staining at intervals up to 9 days following exposure to 8 Gy IR (Figure 5B). To our surprise, all mice examined showed a dramatic decrease in cellularity at 1 and 3 days following irradiation, to the point where the three genotypes were phenotypically indistinguishable. Although WT bone marrow continued to display a progressive loss of cellularity at day 6 after IR, large colonies of cells had appeared in the bone marrow of *Mdm2*^{S394A} and *p53*$^{-/-}$ mice at this time (Figure 5B, arrows). By 9 days post-IR, the colonies present in *Mdm2*^{S394A} and *p53*$^{-/-}$ mice had expanded significantly and often bridged the medullary cavity, whereas only a few smaller colonies were observed in WT bone marrow. Immunohistochemical staining for CD45 confirmed that the colonies were of hematopoietic origin (data not shown). The timing of the increased bone marrow cellularity in *Mdm2*^{S394A} and *p53*$^{-/-}$ mice (but not in WT mice) is likely significant, as it precedes by 1 day the onset of mortality observed in WT mice treated with 8 Gy IR (Gannon et al., 2012).

It has been shown that mice undergoing hematopoietic recovery produce primarily myeloerythroid cells, and myeloerythroid-restricted progenitors are sufficient to confer radioprotection (Uchida et al., 1994; Na Nakorn et al., 2002). We further characterized the bone marrow colonies by IHC staining for the erythroid marker TER-119 (Figure 5C). Consistent with previous findings, we found that approximately 25% of nucleated bone marrow cells and all mature erythrocytes stained positive for TER-119 in the untreated bone marrow of mice irrespective of their genotype (Kina et al., 2000). However, at 9 days post-8 Gy IR treatment, only the few remaining mature erythrocytes in the WT bone marrow stained positive for TER-119, whereas all of the large colonies present in *Mdm2*^{S394A} and *p53*$^{-/-}$ bone marrow were predominantly TER-119 positive. Thus, the p53-dependant resistance to hematopoietic syndrome observed in *Mdm2*^{S394A} and *p53*$^{-/-}$ mice following whole-body IR is linked to the increased capability of these models to repopulate their erythroid cell compartment.

Radiation Resistance in *Mdm2*^{S394A} Mice Is Governed by Hematopoietic Stem and Progenitor Cells

In order to characterize the cell type responsible for the increase in bone marrow repopulation and subsequent radioresistance observed in *Mdm2*^{S394A} mice, we utilized flow cytometry to examine total bone marrow harvested 24 hr after treatment with IR. No differences were observed in the numbers of lineage-defined, mature hematopoietic cells in untreated WT or *Mdm2*^{S394A} mice (Figure 6A). Furthermore, no differences were observed in the numbers of mature hematopoietic cells in irradiated WT or *Mdm2*^{S394A} bone marrow, save for slightly higher numbers of surviving B cells (p = 0.046) in Mdm2 mutant mice. These results are in keeping with the lack of a histopathological

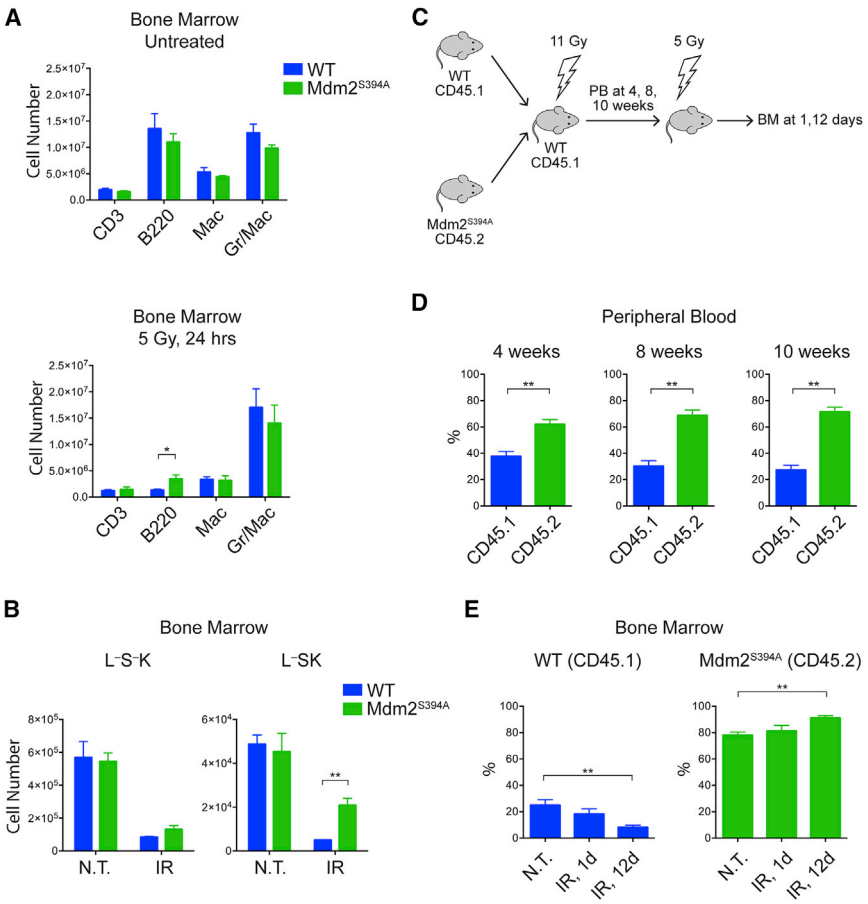

Figure 6. Radiation Resistance in *Mdm2*^{S394A} Mice Is Governed by HSPCs

(A) Quantification of lineage-defined hematopoietic cells in bone marrow of WT and *Mdm2*^{S394A} mice in the absence of treatment (top) and 24 hr after exposure to 5 Gy IR (bottom) (n = 3–4, ± SEM).

(B) Quantification of L$^-$S$^-$K (CMP) and L$^-$SK (HSPC) hematopoietic progenitor cells in bone marrow of WT and *Mdm2*^{S394A} mice described in (A).

(C) Schematic showing the experimental design of bone marrow repopulation assays. PB, peripheral blood; BM, bone marrow.

(D) Leukocyte marker analysis of peripheral blood of recipient mice described in (C) at 4 (n = 15), 8 (n = 15), and 10 (n = 5) weeks after bone marrow transplantation (±SEM).

(E) Leukocyte marker analysis of total bone marrow of recipient mice described in (C), untreated, 1 and 12 days after exposure to 5 Gy IR (n = 5, ± SEM).

*p < 0.05, **p < 0.01 (Student's t tests).

difference in the initial loss of cellularity in irradiated WT and *Mdm2*^{S394A} bone marrow. In addition, no difference was observed in the numbers of Lin−Sca1−cKit+ (L$^-$S$^-$K) common myeloid progenitors (CMPs) in untreated WT and *Mdm2*^{S394A} bone marrow or in WT and *Mdm2*^{S394A} bone marrow following irradiation (Figure 6B). This was confirmed by in vitro colony forming assays performed using the bone marrow of untreated and irradiated WT and *Mdm2*^{S394A} mice (Figure S5). While there was no difference in the numbers of Lin−Sca1+cKit+ (L$^-$SK) hematopoietic stem and progenitor cells (HSPCs) in untreated WT and *Mdm2*^{S394A} bone marrow, there were significantly more HSPCs present in *Mdm2*^{S394A} bone marrow than in WT bone marrow following irradiation (Figure 6B). This finding indicates that the radioresistance observed in *Mdm2*^{S394A} mice is due to reduced loss and/or increased function of HSPCs in this model following IR exposure.

We further examined the HSPCs of *Mdm2*^{S394A} mice by performing in vivo competitive repopulation assays. *Mdm2*^{S394A} bone marrow expressing the CD45.2 leukocyte marker and WT bone marrow expressing the CD45.1 leukocyte marker were transplanted in a 1:1 ratio into lethally irradiated WT (CD45.1) recipient mice (Figure 6C). Peripheral blood analysis at 4, 8, and 10 weeks following transplantation showed gradually increasing relative contributions to the hematopoietic lineage of *Mdm2*^{S394A} bone marrow (62%, 69%, and 72%, respectively) (Figure 6D). This indicated that *Mdm2*^{S394A} HSPCs have an inherent advantage relative to WT HSPCs in their ability to repopulate the hematopoietic compartment of lethally irradiated mice. In addition, we irradiated a cohort of the same bone marrow-chimeric mice at 8 weeks post-transplantation and assayed the relative contributions of WT and *Mdm2*^{S394A} bone marrow 1 and 12 days later (Figure 6E). Relative contributions of 21% WT and 78% *Mdm2*^{S394A} were observed in the untreated bone marrow of reconstituted mice. No significant changes were observed in the percentages of WT and *Mdm2*^{S394A} bone marrow at 1 day after IR (18% and 81%, respectively). However, a significant shift toward a greater proportion of *Mdm2*^{S394A} bone marrow was observed (8% WT, 91% *Mdm2*^{S394A}) in the reconstituted mice 12 days after IR. These results confirm that *Mdm2*^{S394A} HSPCs have a greater capacity to repopulate irradiated bone marrow and determine that *Mdm2*^{S394A} HSPCs display greater stem cell function after genotoxic insult. Furthermore, increased *Mdm2*^{S394A} HSPC cell function is cell-autonomous, as *Mdm2*^{S394A} HSPCs outperform WT HSPCs in a WT microenvironment.

DISCUSSION

Upon exposure to ionizing radiation, the activated ATM effector kinase induces the phosphorylation of multiple signaling molecules involved in the DDR, including the p53 tumor suppressor protein and its chief negative regulator, Mdm2. This signaling cascade has been proposed by many groups to activate p53 by interrupting Mdm2 inhibition of p53, thereby facilitating p53 transactivation of downstream target genes whose products manifest the cellular response to DNA damage. Previously, we

have shown that phosphorylation of p53 serine 18 in mice following DNA damage has only a modest role in regulating p53-mediated apoptosis and in governing p53 tumor suppression, whereas ATM phosphorylation of Mdm2 serine 394 following DNA damage regulates the amplitude and the duration of the DDR in mice and alters p53 suppression of spontaneous tumorigenesis (Sluss et al., 2004; Gannon et al., 2012). These studies demonstrate in vivo the importance of Mdm2 phosphorylation in ATM regulation of the p53 DDR.

In our present study, we explore in vivo the mechanism by which Mdm2 phosphorylation alters p53 functions and examine whether ATM-Mdm2-p53 signaling regulates tumorigenesis in mice induced by activated oncogenes or ionizing radiation. Mdm2 is present at higher levels in the thymus and spleen of *Mdm2*^{S394A} mice following DNA damage (Figures 1A, 2A, and S1). These elevated Mdm2 levels are the result of Mdm2^{S394A} being more stable following DNA damage (Figure 2C), as Mdm2 transcript levels are equivalent or even slightly reduced in IR-treated *Mdm2*^{S394A} tissues during this time frame (Figure 1C). Although we previously found no difference in the stability of phosphorylated Mdm2 after DNA damage (Gannon et al., 2012), using newer and well-validated Mdm2 antibodies and reduced radiation dosages (to promote recovery of the damaged cells), we now find that Mdm2-S394 phosphorylation indeed destabilizes Mdm2 in vivo. Our result is in keeping with previous in vitro studies that indicate a decrease in the half-life of Mdm2 after genotoxic stress (Stommel and Wahl, 2004; Itahana et al., 2007; Inuzuka et al., 2010). Our data provide direct, in vivo evidence that DNA-damage-induced phosphorylation of Mdm2 at this single residue by ATM induces Mdm2 destabilization. Furthermore, our data indicate that Mdm2 levels are elevated in thymi and spleens of *Mdm2*^{S394A} mice even in the absence of acute, exogenous DNA damage (Figures 1A and S1). We interpret this finding to be indicative of some basal level of ATM activity in unstressed tissues that exerts influence on native Mdm2 protein stability.

It is presently unclear how Mdm2 phosphorylation facilitates Mdm2 destabilization. DNA-damage-induced degradation of Mdm2 has been shown to occur even in the absence of Mdm2 E3 ligase activity (Itahana et al., 2007), and studies have identified the F-box proteins β-TRCP and FBXO31 as mediators of Mdm2 degradation by the SCF complex (Inuzuka et al., 2010; Malonia et al., 2015). Since FBXO31 is phosphorylated by ATM and was recently found to interact with Mdm2 in a manner dependent on ATM phosphorylation of Mdm2 (Santra et al., 2009; Malonia et al., 2015), it is plausible that ATM phosphorylation of Mdm2-S394 in IR-treated mice results in FBXO31-induced destabilization of Mdm2. Unfortunately, our attempts to assay Mdm2-FBXO31 interactions in whole tissues before and after DNA damage have proven unsuccessful. Thus, the precise mechanism of how ATM phosphorylation of Mdm2-S394 promotes Mdm2 degradation under physiologic conditions remains to be determined.

The increased levels of Mdm2 observed in the spleen and thymus of *Mdm2*^{S394A} mice after DNA damage correlate with decreased p53 levels and p53 activity in these *Mdm2*^{S394A} tissues. Previous studies have suggested that ATM phosphorylation of the analogous residue on human MDM2 (S395), either alone or in combination with several other ATM-target serine residues in the same region, impacts Mdm2's ability to promote p53 degradation and nuclear export and governs RING-domain oligomerization and polyubiquitination of p53 (Maya et al., 2001; Cheng et al., 2009). DNA damage resulted in p53 stabilization in WT thymocytes, albeit after a brief period of p53 degradation (Figure S2B). While the initial rate of p53 degradation does not appear affected in irradiated *Mdm2*^{S394A} thymocytes, we observed a prolonged period of p53 destabilization, ultimately resulting in lower relative levels of p53. This prolonged p53 destabilization may reflect the increased stability of Mdm2^{S394A} after DNA damage. This is supported by the increased relative amounts of Mdm2-bound p53 after IR observed in *Mdm2*^{S394A} thymi (Figure 2C). However, it remains possible that increased DNA-damage-induced p53 activity in WT thymi is caused not only by reduced Mdm2-mediated p53 degradation (due to destabilization of Mdm2) but also by reduced Mdm2 steric inhibition of p53. As Mdm2 binds to the amino-terminal, transcriptional activation domain of p53 and inhibits p53 target gene expression, reduced Mdm2-p53 complex formation after Mdm2 phosphorylation by ATM may account for the increase in p53 activity even when p53 protein stability is only modestly altered (Momand et al., 1992; Oliner et al., 1993).

The reduced level of p53 activity in *Mdm2*^{S394A} mice facilitates more rapid B cell lymphomagenesis in *Eμ-myc* mice (Figure 3). It has been previously demonstrated that activated oncogenes such as *Myc* result in elevated Arf expression, a result of hyperproliferative signaling (Zindy et al., 1998; Sherr et al., 2005). The importance of disrupting the Arf-Mdm2-p53 pathway in Myc-driven lymphomagenesis is evidenced by the fact that *Eμ-myc* driven tumors in mice face a selective pressure to inactivate the p53 pathway, by either p53 mutation, Mdm2 overexpression, or loss of Arf (Eischen et al., 1999). However, we observed a significant acceleration in the median time of tumor presentation in *Eμ-myc;Mdm2*^{S394A} mice in the absence of Mdm2 overexpression or p53 mutation in tumors (Figures 3A and 3C). This suggests that an absence of Mdm2-S394 phosphorylation is sufficient to diminish p53 activity in response to oncogene activation and reduces the selective pressure to genetically disrupt the Mdm2-p53 signaling axis (Figure 3D). Although loss of Arf was observed in a subset of *Eμ-myc;Mdm2*^{S394A} tumors, this finding likely reflects the ability of Arf to prevent tumorigenesis in *Eμ-myc* mice through an Mdm2/p53 independent mechanism.

Although elevated Myc levels have been shown to result in increased levels of cellular DNA damage, the relative contributions of the pro-proliferative effects and DNA-damage-induced effects of Myc on tumor formation remain uncertain (Halazonetis et al., 2008; Meek, 2015). To further explore a role for Mdm2 phosphorylation in the DDR and in regulation of p53 tumor suppression, we examined lymphomagenesis induced by low level exposure of mice to ionizing radiation (Figure 4). In contrast to our results in Myc-driven lymphomagenesis, *Mdm2*^{S394A} mice proved to be more resistant to DNA-damage-induced T cell lymphomagenesis, highlighting a stark difference in the effects of ATM-Mdm2-p53 signaling in lymphomas induced by different types of DNA-damage-related stress.

The cell of origin in IR-induced lymphomas has historically been viewed as a stem and/or progenitor cell residing within

the bone marrow (Kaplan, 1964), and IR-induced lymphomagenesis is significantly enhanced in the absence of functional p53 (Kemp et al., 1994). Subsequent studies examining the contribution of the p53-dependent pro-apoptotic genes *Puma* and *Noxa* made the paradoxical observation that *Puma*$^{-/-}$ mice develop fewer IR-induced lymphomas (Labi et al., 2010; Michalak et al., 2010). This was attributed to increased survival of leukocytes in the bone marrow, which reduced the proliferative stress and/or propagation of lesions within progenitor cells tasked with repopulating the bone marrow. That *Noxa*$^{-/-}$ mice displayed only modest radioprotection of LSK cells and developed more lymphomas was interpreted as a failure to clear damaged progenitors, thereby promoting the survival of damaged stem and/or progenitor cells (Michalak et al., 2010). Despite a reduction of p53-dependent gene expression of *Puma* and *Noxa* in total bone marrow of IR-damaged *Mdm2*^{S394} mice (Figure 5A), we observed no defects in the attrition of mature hematopoietic cells or lineage-defined progenitor cells (CMPs) (Figures 6A and 6B). Only the most primitive HSPCs display resistance to IR (Figure 6B). Our finding that *Mdm2*^{S394A} mice are resistant to IR-induced lymphomas reveals that the effects of a reduced p53-dependent damage response in *Mdm2*^{S394A} mice does not mirror the ablation of either *Puma* or *Noxa* alone. Interestingly, a recent study by Lee et al. (2015) suggests that the tumor-initiating cell in IR-induced lymphomas is thymic in origin. Using mice in which p53 activity was temporally blocked during total-body irradiation, the authors propose that the IR-induced p53 response in bone marrow promotes lymphomagenesis by reducing HSPC fitness, thereby reducing the competition of cells originating from the bone marrow with thymocytes containing oncogenic lesions. The results we have observed with *Mdm2*^{S394A} mice align favorably with this model, as we have observed less p53 activity and increased HSPC fitness in *Mdm2*^{S394A} mice following threshold-lethal doses of radiation and observed reduced incidence of T cell lymphomagenesis in *Mdm2*^{S394A} mice after IR exposure (Figures 5 and 6). The p53 dependence of the increased HSPC fitness in *Mdm2*^{S394A} mice is further intimated by studies that have observed increased bone marrow repopulation potential in bone marrow deficient for p53, both in the presence and absence of IR (reviewed in Pant et al., 2012). Interestingly, a recent study has linked Mdm2 to enhanced stem-ness via association with the Polycomb Repressor Complex 2 (PRC2) (Wienken et al., 2016). Further studies into the relative p53-dependent and p53-independent contributions of Mdm2 to HSPC fitness are clearly warranted.

We conclude that ATM phosphorylation of Mdm2-S394 is critical for Mdm2 degradation and robust p53 activation after DNA damage. Our results show that while ATM's regulation of p53 activity through Mdm2 is critical in preventing oncogene-induced tumorigenesis, disrupting this regulation imparts protection from bone marrow ablation and lymphomagenesis resulting after DNA damage. These observations are of clinical significance, as they suggest that the temporal inhibition of Mdm2 phosphorylation by short-acting kinase inhibitors or by use of excess decoy ATM target-sites (a molecular sponge of sorts) would reduce p53 activation and alleviate the toxicity associated with radiotherapies. Our results further indicate that such treatment would likely protect against the subsequent development of secondary hematological malignancies induced by exposure to ionizing radiation.

EXPERIMENTAL PROCEDURES

Mice and Animal Studies

All animals described in this study were on a C57Bl/6 background. Mice and cells were irradiated with a cesium-137 source (Gammacell 40). The generation of *Mdm2*^{S394A} mice has been previously described (Gannon et al., 2012). *Eμ-Myc* mice were a gift from Christine Eischen (Vanderbilt University). Mice in *Eμ-Myc* tumor assays were virgin and inherited the *Eμ-Myc* allele paternally. For IR-induced tumor assays, mice 31 ± 3 days of age were irradiated weekly with 1.75 Gy for 4 weeks (7 Gy cumulative dose). For bone marrow transplantation experiments, recipient CD45.1 mice received 11 Gy of whole-body irradiation in a split dose (2 × 5.5 Gy, 4 hr apart). Irradiated recipients were reconstituted by intravenous (i.v.) injection of 2 × 10^6 bone marrow cells (1:1 mixture of WT and *Mdm2*^{S394A}). All animals used in this study were maintained and assayed in accordance with federal guidelines and those established by the Institutional Animal Care and Use Committee at the University of Massachusetts Medical School.

Protein Analysis

Tissues and cells were lysed in NP-40 lysis buffer or in CelLytic MT Cell Lysis Reagent (Sigma), supplemented with protease and phosphatase inhibitors. Protein extracts were analyzed by western blotting or immunoprecipitation and western blotting. A detailed description of the methods employed, including antibodies and clones, is provided in the Supplemental Experimental Procedures.

Gene Expression Analysis and Sequencing

Total RNA was isolated from tissues by RNeasy mini kit (QIAGEN) and cDNA synthesized by Superscript III First Strand Synthesis System (Invitrogen). qPCR was performed using SYBR Select Master Mix (Applied Biosystems) in conjunction with a 7300 Real-Time PCR System (Applied Biosystems). A detailed description of the methods employed, including primer sequences, for qPCR, RT-PCR, and sequencing is provided in the Supplemental Experimental Procedures.

Histopathology

Tissues samples were fixed in 10% formalin for 24 hr. The UMMS Diabetes and Endocrinology Research Center Morphology Core performed embedding, sectioning, and staining. TUNEL staining was performed using the In Situ Cell Death Detection Kit, POD (Roche), according to manufacturer's instructions. IHC was performed with antibodies specific for B220 (550286; BD Pharmingen), CD3 (A0452; Dako), and TER-119 (553671; BD Pharmingen). Stained tissue was analyzed using an Olympus CX41 microscope fitted with a PixeLINK camera and software.

Flow Cytometry

Total bone marrow from both hind limbs was harvested, red blood cells were lysed, and single-cell suspensions were stained with cell-surface antibodies for Gr-1, CD11B, CD3, and B220. For LSK analysis, bone marrow cells were stained with a biotin lineage mixture and were stained with antibodies for Sca-1, c-Kit, CD34, and Flk2. To distinguish between WT and *Mdm2*^{S394A} hematopoietic cells in the reconstitution studies, peripheral blood and bone marrow were stained with antibodies specific for CD45.1 and CD45.2. All samples were run on a BD LSRII flow cytometer (BD Bioscience) and analyzed using FlowJo software (Tree Star). A complete list of antibodies including clone numbers is given in Table S1.

Statistical Analysis

Statistical analyses were performed using GraphPad Prism software v.6.0d. Kaplan-Meier survival curves were analyzed by log rank test. A p value of <0.05 was considered statistically significant for Student's t tests.

SUPPLEMENTAL INFORMATION

Supplemental Information includes Supplemental Experimental Procedures, five figures, and one table and can be found with this article online at http://dx.doi.org/10.1016/j.celrep.2016.08.014.

AUTHOR CONTRIBUTIONS

Conceptualization, M.I.C. and S.N.J.; Methodology, M.I.C., H.S.G., and S.N.J.; Investigation, M.I.C. and J.E.R.; Resources, M.A.K. and S.N.J.; Writing – Original Draft, M.I.C. and S.N.J.; Writing – Review & Editing, M.I.C., J.E.R., H.S.G., M.A.K., and S.N.J.; Funding Acquisition, S.N.J.

ACKNOWLEDGMENTS

This research was supported by the following grants from the NIH: R01-CA077735 (S.N.J.) and R01-CA096899 (M.A.K.). J.E.R. was supported by postdoctoral fellowship 125087-PF-13-247-01-LIB from the American Cancer Society.

Received: April 16, 2016
Revised: June 17, 2016
Accepted: August 3, 2016
Published: August 25, 2016

REFERENCES

Adams, J.M., Harris, A.W., Pinkert, C.A., Corcoran, L.M., Alexander, W.S., Cory, S., Palmiter, R.D., and Brinster, R.L. (1985). The c-myc oncogene driven by immunoglobulin enhancers induces lymphoid malignancy in transgenic mice. Nature *318*, 533–538.

Beckerman, R., and Prives, C. (2010). Transcriptional regulation by p53. Cold Spring Harb. Perspect. Biol. *2*, a000935.

Brady, C.A., Jiang, D., Mello, S.S., Johnson, T.M., Jarvis, L.A., Kozak, M.M., Kenzelmann Broz, D., Basak, S., Park, E.J., McLaughlin, M.E., et al. (2011). Distinct p53 transcriptional programs dictate acute DNA-damage responses and tumor suppression. Cell *145*, 571–583.

Chao, C., Hergenhahn, M., Kaeser, M.D., Wu, Z., Saito, S., Iggo, R., Hollstein, M., Appella, E., and Xu, Y. (2003). Cell type- and promoter-specific roles of Ser18 phosphorylation in regulating p53 responses. J. Biol. Chem. *278*, 41028–41033.

Chao, C., Herr, D., Chun, J., and Xu, Y. (2006). Ser18 and 23 phosphorylation is required for p53-dependent apoptosis and tumor suppression. EMBO J. *25*, 2615–2622.

Chen, L., Gilkes, D.M., Pan, Y., Lane, W.S., and Chen, J. (2005). ATM and Chk2-dependent phosphorylation of MDMX contribute to p53 activation after DNA damage. EMBO J. *24*, 3411–3422.

Cheng, T., Rodrigues, N., Shen, H., Yang, Y., Dombkowski, D., Sykes, M., and Scadden, D.T. (2000). Hematopoietic stem cell quiescence maintained by p21cip1/waf1. Science *287*, 1804–1808.

Cheng, Q., Chen, L., Li, Z., Lane, W.S., and Chen, J. (2009). ATM activates p53 by regulating MDM2 oligomerization and E3 processivity. EMBO J. *28*, 3857–3867.

Cheng, Q., Cross, B., Li, B., Chen, L., Li, Z., and Chen, J. (2011). Regulation of MDM2 E3 ligase activity by phosphorylation after DNA damage. Mol. Cell. Biol. *31*, 4951–4963.

Donehower, L.A., Harvey, M., Slagle, B.L., McArthur, M.J., Montgomery, C.A.J., Jr., Butel, J.S., and Bradley, A. (1992). Mice deficient for p53 are developmentally normal but susceptible to spontaneous tumours. Nature *356*, 215–221.

Eischen, C.M., Weber, J.D., Roussel, M.F., Sherr, C.J., and Cleveland, J.L. (1999). Disruption of the ARF-Mdm2-p53 tumor suppressor pathway in Myc-induced lymphomagenesis. Genes Dev. *13*, 2658–2669.

Gannon, H.S., and Jones, S.N. (2012). Using mouse models to explore MDM-p53 signaling in development, cell growth, and tumorigenesis. Genes Cancer *3*, 209–218.

Gannon, H.S., Woda, B.A., and Jones, S.N. (2012). ATM phosphorylation of Mdm2 Ser394 regulates the amplitude and duration of the DNA damage response in mice. Cancer Cell *21*, 668–679.

Halazonetis, T.D., Gorgoulis, V.G., and Bartek, J. (2008). An oncogene-induced DNA damage model for cancer development. Science *319*, 1352–1355.

Haupt, Y., Maya, R., Kazaz, A., and Oren, M. (1997). Mdm2 promotes the rapid degradation of p53. Nature *387*, 296–299.

Honda, R., Tanaka, H., and Yasuda, H. (1997). Oncoprotein MDM2 is a ubiquitin ligase E3 for tumor suppressor p53. FEBS Lett. *420*, 25–27.

Huang, L., Yan, Z., Liao, X., Li, Y., Yang, J., Wang, Z.-G., Zuo, Y., Kawai, H., Shadfan, M., Ganapathy, S., and Yuan, Z.M. (2011). The p53 inhibitors MDM2/MDMX complex is required for control of p53 activity in vivo. Proc. Natl. Acad. Sci. USA *108*, 12001–12006.

Inuzuka, H., Tseng, A., Gao, D., Zhai, B., Zhang, Q., Shaik, S., Wan, L., Ang, X.L., Mock, C., Yin, H., et al. (2010). Phosphorylation by casein kinase I promotes the turnover of the Mdm2 oncoprotein via the SCF(β-TRCP) ubiquitin ligase. Cancer Cell *18*, 147–159.

Itahana, K., Mao, H., Jin, A., Itahana, Y., Clegg, H.V., Lindström, M.S., Bhat, K.P., Godfrey, V.L., Evan, G.I., and Zhang, Y. (2007). Targeted inactivation of Mdm2 RING finger E3 ubiquitin ligase activity in the mouse reveals mechanistic insights into p53 regulation. Cancer Cell *12*, 355–366.

Jackson, M.W., and Berberich, S.J. (2000). MdmX protects p53 from Mdm2-mediated degradation. Mol. Cell. Biol. *20*, 1001–1007.

Jones, S.N., Roe, A.E., Donehower, L.A., and Bradley, A. (1995). Rescue of embryonic lethality in Mdm2-deficient mice by absence of p53. Nature *378*, 206–208.

Kaplan, H.S. (1964). The role of radiation on experimental leukemogenesis. Natl. Cancer Inst. Monogr. *14*, 207–220.

Kaplan, H.S., and Brown, M.B. (1952). A quantitative dose-response study of lymphoid-tumor development in irradiated C 57 black mice. J. Natl. Cancer Inst. *13*, 185–208.

Kawai, H., Lopez-Pajares, V., Kim, M.M., Wiederschain, D., and Yuan, Z.-M. (2007). RING domain-mediated interaction is a requirement for MDM2's E3 ligase activity. Cancer Res. *67*, 6026–6030.

Kemp, C.J., Wheldon, T., and Balmain, A. (1994). p53-deficient mice are extremely susceptible to radiation-induced tumorigenesis. Nat. Genet. *8*, 66–69.

Kina, T., Ikuta, K., Takayama, E., Wada, K., Majumdar, A.S., Weissman, I.L., and Katsura, Y. (2000). The monoclonal antibody TER-119 recognizes a molecule associated with glycophorin A and specifically marks the late stages of murine erythroid lineage. Br. J. Haematol. *109*, 280–287.

Komarova, E.A., Kondratov, R.V., Wang, K., Christov, K., Golovkina, T.V., Goldblum, J.R., and Gudkov, A.V. (2004). Dual effect of p53 on radiation sensitivity in vivo: p53 promotes hematopoietic injury, but protects from gastro-intestinal syndrome in mice. Oncogene *23*, 3265–3271.

Kubbutat, M.H.G., Jones, S.N., and Vousden, K.H. (1997). Regulation of p53 stability by Mdm2. Nature *387*, 299–303.

Labi, V., Erlacher, M., Krumschnabel, G., Manzl, C., Tzankov, A., Pinon, J., Egle, A., and Villunger, A. (2010). Apoptosis of leukocytes triggered by acute DNA damage promotes lymphoma formation. Genes Dev. *24*, 1602–1607.

Lee, C.-L., Castle, K.D., Moding, E.J., Blum, J.M., Williams, N., Luo, L., Ma, Y., Borst, L.B., Kim, Y., and Kirsch, D.G. (2015). Acute DNA damage activates the tumour suppressor p53 to promote radiation-induced lymphoma. Nat. Commun. *6*, 8477.

Li, T., Kon, N., Jiang, L., Tan, M., Ludwig, T., Zhao, Y., Baer, R., and Gu, W. (2012). Tumor suppression in the absence of p53-mediated cell-cycle arrest, apoptosis, and senescence. Cell *149*, 1269–1283.

Malonia, S.K., Dutta, P., Santra, M.K., and Green, M.R. (2015). F-box protein FBXO31 directs degradation of MDM2 to facilitate p53-mediated growth arrest following genotoxic stress. Proc. Natl. Acad. Sci. USA *112*, 8632–8637.

Maya, R., Balass, M., Kim, S.-T., Shkedy, D., Leal, J.-F.M., Shifman, O., Moas, M., Buschmann, T., Ronai, Z., Shiloh, Y., et al. (2001). ATM-dependent phosphorylation of Mdm2 on serine 395: role in p53 activation by DNA damage. Genes Dev. *15*, 1067–1077.

Meek, D.W. (2015). Regulation of the p53 response and its relationship to cancer. Biochem. J. *469*, 325–346.

Mendrysa, S.M., McElwee, M.K., Michalowski, J., O'Leary, K.A., Young, K.M., and Perry, M.E. (2003). mdm2 Is critical for inhibition of p53 during lymphopoiesis and the response to ionizing irradiation. Mol. Cell. Biol. *23*, 462–472.

Michalak, E.M., Vandenberg, C.J., Delbridge, A.R.D., Wu, L., Scott, C.L., Adams, J.M., and Strasser, A. (2010). Apoptosis-promoted tumorigenesis: γ-irradiation-induced thymic lymphomagenesis requires Puma-driven leukocyte death. Genes Dev. *24*, 1608–1613.

Migliorini, D., Lazzerini Denchi, E., Danovi, D., Jochemsen, A., Capillo, M., Gobbi, A., Helin, K., Pelicci, P.G., and Marine, J.-C. (2002). Mdm4 (Mdmx) regulates p53-induced growth arrest and neuronal cell death during early embryonic mouse development. Mol. Cell. Biol. *22*, 5527–5538.

Momand, J., Zambetti, G.P., Olson, D.C., George, D., and Levine, A.J. (1992). The mdm-2 oncogene product forms a complex with the p53 protein and inhibits p53-mediated transactivation. Cell *69*, 1237–1245.

Montes de Oca Luna, R., Wagner, D.S., and Lozano, G. (1995). Rescue of early embryonic lethality in mdm2-deficient mice by deletion of p53. Nature *378*, 203–206.

Na Nakorn, T., Traver, D., Weissman, I.L., and Akashi, K. (2002). Myeloerythroid-restricted progenitors are sufficient to confer radioprotection and provide the majority of day 8 CFU-S. J. Clin. Invest. *109*, 1579–1585.

Oliner, J.D., Pietenpol, J.A., Thiagalingam, S., Gyuris, J., Kinzler, K.W., and Vogelstein, B. (1993). Oncoprotein MDM2 conceals the activation domain of tumour suppressor p53. Nature *362*, 857–860.

Pant, V., Xiong, S., Iwakuma, T., Quintás-Cardama, A., and Lozano, G. (2011). Heterodimerization of Mdm2 and Mdm4 is critical for regulating p53 activity during embryogenesis but dispensable for p53 and Mdm2 stability. Proc. Natl. Acad. Sci. USA *108*, 11995–12000.

Pant, V., Quintás-Cardama, A., and Lozano, G. (2012). The p53 pathway in hematopoiesis: lessons from mouse models, implications for humans. Blood *120*, 5118–5127.

Pant, V., Xiong, S., Jackson, J.G., Post, S.M., Abbas, H.A., Quintás-Cardama, A., Hamir, A.N., and Lozano, G. (2013). The p53-Mdm2 feedback loop protects against DNA damage by inhibiting p53 activity but is dispensable for p53 stability, development, and longevity. Genes Dev. *27*, 1857–1867.

Parant, J., Chavez-Reyes, A., Little, N.A., Yan, W., Reinke, V., Jochemsen, A.G., and Lozano, G. (2001). Rescue of embryonic lethality in Mdm4-null mice by loss of Trp53 suggests a nonoverlapping pathway with MDM2 to regulate p53. Nat. Genet. *29*, 92–95.

Pereg, Y., Shkedy, D., de Graaf, P., Meulmeester, E., Edelson-Averbukh, M., Salek, M., Biton, S., Teunisse, A.F.A.S., Lehmann, W.D., Jochemsen, A.G., and Shiloh, Y. (2005). Phosphorylation of Hdmx mediates its Hdm2- and ATM-dependent degradation in response to DNA damage. Proc. Natl. Acad. Sci. USA *102*, 5056–5061.

Santra, M.K., Wajapeyee, N., and Green, M.R. (2009). F-box protein FBXO31 mediates cyclin D1 degradation to induce G1 arrest after DNA damage. Nature *459*, 722–725.

Shao, L., Sun, Y., Zhang, Z., Feng, W., Gao, Y., Cai, Z., Wang, Z.Z., Look, A.T., and Wu, W.-S. (2010). Deletion of proapoptotic Puma selectively protects hematopoietic stem and progenitor cells against high-dose radiation. Blood *115*, 4707–4714.

Sharp, D.A., Kratowicz, S.A., Sank, M.J., and George, D.L. (1999). Stabilization of the MDM2 oncoprotein by interaction with the structurally related MDMX protein. J. Biol. Chem. *274*, 38189–38196.

Sherr, C.J., Bertwistle, D., DEN Besten, W., Kuo, M.-L., Sugimoto, M., Tago, K., Williams, R.T., Zindy, F., and Roussel, M.F. (2005). p53-Dependent and -independent functions of the Arf tumor suppressor. Cold Spring Harb. Symp. Quant. Biol. *70*, 129–137.

Shieh, S.-Y., Ikeda, M., Taya, Y., and Prives, C. (1997). DNA damage-induced phosphorylation of p53 alleviates inhibition by MDM2. Cell *91*, 325–334.

Shieh, S.-Y., Ahn, J., Tamai, K., Taya, Y., and Prives, C. (2000). The human homologs of checkpoint kinases Chk1 and Cds1 (Chk2) phosphorylate p53 at multiple DNA damage-inducible sites. Genes Dev. *14*, 289–300.

Shvarts, A., Steegenga, W.T., Riteco, N., van Laar, T., Dekker, P., Bazuine, M., van Ham, R.C., van der Houven van Oordt, W., Hateboer, G., van der Eb, A.J., and Jochemsen, A.G. (1996). MDMX: a novel p53-binding protein with some functional properties of MDM2. EMBO J. *15*, 5349–5357.

Sluss, H.K., Armata, H., Gallant, J., and Jones, S.N. (2004). Phosphorylation of serine 18 regulates distinct p53 functions in mice. Mol. Cell. Biol. *24*, 976–984.

Sluss, H.K., Gannon, H., Coles, A.H., Shen, Q., Eischen, C.M., and Jones, S.N. (2010). Phosphorylation of p53 serine 18 upregulates apoptosis to suppress Myc-induced tumorigenesis. Mol. Cancer Res. *8*, 216–222.

Soussi, T., and Béroud, C. (2001). Assessing TP53 status in human tumours to evaluate clinical outcome. Nat. Rev. Cancer *1*, 233–240.

Stommel, J.M., and Wahl, G.M. (2004). Accelerated MDM2 auto-degradation induced by DNA-damage kinases is required for p53 activation. EMBO J. *23*, 1547–1556.

Tanimura, S., Ohtsuka, S., Mitsui, K., Shirouzu, K., Yoshimura, A., and Ohtsubo, M. (1999). MDM2 interacts with MDMX through their RING finger domains. FEBS Lett. *447*, 5–9.

Terzian, T., Wang, Y., Van Pelt, C.S., Box, N.F., Travis, E.L., and Lozano, G. (2007). Haploinsufficiency of Mdm2 and Mdm4 in tumorigenesis and development. Mol. Cell. Biol. *27*, 5479–5485.

Tollini, L.A., Jin, A., Park, J., and Zhang, Y. (2014). Regulation of p53 by Mdm2 E3 ligase function is dispensable in embryogenesis and development, but essential in response to DNA damage. Cancer Cell *26*, 235–247.

Uchida, N., Aguila, H.L., Fleming, W.H., Jerabek, L., and Weissman, I.L. (1994). Rapid and sustained hematopoietic recovery in lethally irradiated mice transplanted with purified Thy-1.1lo Lin-Sca-1+ hematopoietic stem cells. Blood *83*, 3758–3779.

van Os, R., Kamminga, L.M., Ausema, A., Bystrykh, L.V., Draijer, D.P., van Pelt, K., Dontje, B., and de Haan, G. (2007). A limited role for p21Cip1/Waf1 in maintaining normal hematopoietic stem cell functioning. Stem Cells *25*, 836–843.

Wang, Y.V., Leblanc, M., Wade, M., Jochemsen, A.G., and Wahl, G.M. (2009). Increased radioresistance and accelerated B cell lymphomas in mice with Mdmx mutations that prevent modifications by DNA-damage-activated kinases. Cancer Cell *16*, 33–43.

Wang, Y.V., Leblanc, M., Fox, N., Mao, J.-H., Tinkum, K.L., Krummel, K., Engle, D., Piwnica-Worms, D., Piwnica-Worms, H., Balmain, A., et al. (2011). Fine-tuning p53 activity through C-terminal modification significantly contributes to HSC homeostasis and mouse radiosensitivity. Genes Dev. *25*, 1426–1438.

Wienken, M., Dickmanns, A., Nemajerova, A., Kramer, D., Najafova, Z., Weiss, M., Karpiuk, O., Kassem, M., Zhang, Y., Lozano, G., et al. (2016). MDM2 associates with Polycomb Repressor Complex 2 and enhances stemness-promoting chromatin modifications independent of p53. Mol. Cell *61*, 68–83.

Wu, Z., Earle, J., Saito, S., Anderson, C.W., Appella, E., and Xu, Y. (2002). Mutation of mouse p53 Ser23 and the response to DNA damage. Mol. Cell. Biol. *22*, 2441–2449.

Yu, H., Shen, H., Yuan, Y., XuFeng, R., Hu, X., Garrison, S.P., Zhang, L., Yu, J., Zambetti, G.P., and Cheng, T. (2010). Deletion of Puma protects hematopoietic stem cells and confers long-term survival in response to high-dose γ-irradiation. Blood *115*, 3472–3480.

Zindy, F., Eischen, C.M., Randle, D.H., Kamijo, T., Cleveland, J.L., Sherr, C.J., and Roussel, M.F. (1998). Myc signaling via the ARF tumor suppressor regulates p53-dependent apoptosis and immortalization. Genes Dev. *12*, 2424–2433.